EPJ Web of Conferences **274**, 02011 (2022) https://doi.org/10.1051/epjconf/202227402011
XVth Quark Confinement and the Hadron Spectrum

Field, current, and charge distribution in a pure gauge SU(3) flux tube

Marshall Baker[1,*], *Volodymyr* Chelnokov[2,**], *Leonardo* Cosmai[3,***], *Francesca* Cuteri[2,****], and *Alessandro* Papa[4,5,†]

[1]Department of Physics, University of Washington, WA 98105 Seattle, USA
[2]Institut für Theoretische Physik, Goethe Universität, 60438 Frankfurt am Main, Germany
[3]INFN - Sezione di Bari, I-70126 Bari, Italy
[4]Dipartimento di Fisica, Università della Calabria, I-87036 Arcavacata di Rende, Cosenza, Italy
[5]INFN - Gruppo collegato di Cosenza, I-87036 Arcavacata di Rende, Cosenza, Italy

Abstract. The quark confinement in QCD is achieved by concentration of the chromoelectric field between the quark-antiquark pair into a flux tube, which gives rise to a linear quark-antiquark potential. We study the structure of the flux tube created by a static quark-antiquark pair in the pure gauge SU(3) theory, using lattice Monte-Carlo simulations. We calculate the spatial distribution of all three components of the chromoelectric field and perform the "zero curl subtraction" procedure to obtain the nonperturbative part of the longitudinal component of the field, which we identify as the part responsible for the formation of the flux tube. Taking the spatial derivatives of the obtained field allows us to extract the electric charge and magnetic current densities in the flux tube. The behavior of these observables under smearing and with respect to continuum scaling is investigated. Finally, we briefly discuss the role of magnetic currents in the formation of the string tension.

1 Introduction

Color confinement remains an open problem of Quantum Chromodynamics (QCD). A strict analytical proof of confinement is still missing not only for full QCD, but also for the pure gauge SU(2) or SU(3) theories. Moreover, there is no clear agreement on the features of the theory that is responsible for the confinement. A review of the confinement problem in QCD can be found in [1].

A large number of numerical studies provide evidence of confinement both in pure gauge SU(2) and SU(3) theories [2–29], and, more recently, in full QCD [30–33]. From these studies, we know that at temperatures below the deconfinement temperature $T_{\rm dec}$, the interaction between a static quark and antiquark is governed by a linear potential, that is observed for quark-antiquark separation $d \geq 0.5$ fm. For the pure gauge theories, this linear potential extends to arbitrarily large d, while in full QCD it extends up to $d \approx 1.4$ fm, where string

*e-mail: mbaker4@uw.edu
**e-mail: chelnokov@itp.uni-frankfurt.de
***e-mail: leonardo.cosmai@ba.infn.it
****e-mail: cuteri@itp.uni-frankfurt.de
†e-mail: alessandro.papa@fis.unical.it

breaking takes place due to the screening of the potential by dynamical quarks [34–37]. The chromoelectric field of the quark-antiquark pair is concentrated in a tube-like structure, where the field is mainly longitudinal i.e. aligned with the quark-antiquark axis. This structure is called a "flux tube" and the energy density of the field in it gives rise to a linear quark-antiquark potential

We report on our studies of the spatial structure of the field in pure gauge SU(3) flux tube created by a static quark-antiquark pair at zero temperature, and the field derivatives describing the chromoelectric charge density and the chromomagnetic current density. In our previous papers [38, 39], we described the field obtained in the lattice simulation as a sum of the "perturbative" part governing the short-range behavior of the potential, and the "non-perturbative" part that is strictly aligned with the quark-antiquark axis, the flux tube being identified with the nonperturbative field part. Here we extend the analysis with a calculation of the derivatives of the "nonperturbative" field. A more detailed description of our latest results can be found in [40].

2 Observables and lattice setup

We simulated pure SU(3) lattice gauge theory with standard Wilson action in four dimensions, using the publicly available MILC code, modified to introduce the field observables and the smearing procedure.

We measure the field distributions using a connected correlator $\rho^{\rm conn}_{W,\mu\nu}$ [6, 7, 41] between a plaquette $U_P = U_{\mu\nu}(x)$, lying in the $\mu\nu$ plane, and a Wilson loop W in the $\hat{4}\hat{1}$ plane, connected by a Schwinger line L (see Figure 1),

$$\rho^{\rm conn}_{W,\mu\nu} = \frac{\langle {\rm tr}\,(WLU_PL^*)\rangle}{\langle {\rm tr}\ W\rangle} - \frac{1}{3}\frac{\langle {\rm tr}\ U_P\,{\rm tr}\ W\rangle}{\langle {\rm tr}\ W\rangle}\ . \tag{1}$$

Then the lattice definition of the field strength tensor $F_{\mu\nu}$ is taken as

$$F_{\mu\nu_{\rm lat}} = \frac{1}{ga^2}\rho^{\rm conn}_{W,\mu\nu}\ . \tag{2}$$

The component of the field is defined by the plane $\mu\nu$ of the plaquette U_P. Since we consider the quark-antiquark axis to lie along $\hat{1}$ (x axis), and the transverse displacement to be along $\hat{2}$ (y axis), we can write $E_l \equiv E_x \equiv F_{\hat{4}\hat{1}}$, $E_t \equiv E_y \equiv F_{\hat{4}\hat{2}}$. In practice, the measurements were averaged over all equivalent rotations (relabelings) of the lattice axes to reduce the stochastic noise.

The simulations were performed at three values of the gauge coupling β, with $d = 8a, 12a, 16a$ while keeping the distance in physical units constant (see Table 1). The physical scale for the lattice spacing a was set according to [42],

$$\begin{aligned}
&a(\beta) = r_0 \times \exp\left[c_0 + c_1(\beta-6) + c_2(\beta-6)^2 + c_3(\beta-6)^3\right],\\
&r_0 = 0.5\ {\rm fm},\\
&c_0 = -1.6804\,, c_1 = -1.7331\,,\\
&c_2 = 0.7849\,, c_3 = -0.4428\,.
\end{aligned} \tag{3}$$

To improve the signal-to-noise ratio of the correlator, a smearing procedure was implemented that consisted of one step of 4-dimensional Hypercubic smearing [43] on the temporal links (HYPt), with smearing parameters $(\alpha_1, \alpha_2, \alpha_3) = (1.0, 1.0, 0.5)$, and $N_{\rm HYP3d}$ steps of hypercubic smearing restricted to the three spatial directions (HYP3d) with $(\alpha_1^{\rm HYP3d}, \alpha_3^{\rm HYP3d}) =$

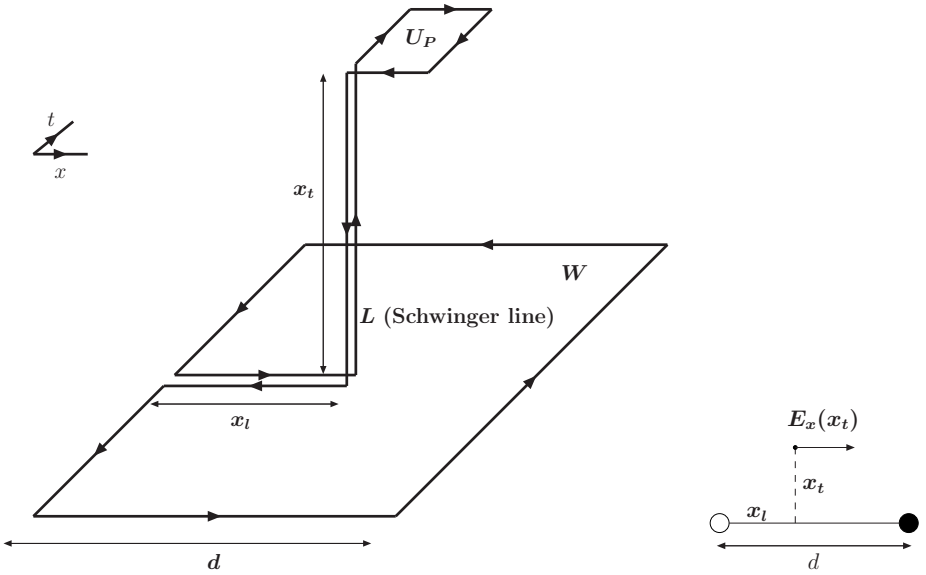

Figure 1. The connected correlator (1) (subtraction in $\rho^{\text{conn}}_{W,\mu\nu}$ not explicitly drawn) and the geometry of the system.

Table 1. Lattice setup.

lattice	$\beta = 6/g^2$	$a(\beta)$ [fm]	d [fm]	statistics
48^4	6.240	0.0639	$8a = 0.511$	268
48^4	6.544	0.0426	$12a = 0.511$	508
48^4	6.769	0.0320	$16a = 0.511$	303

$(0.75, 0.3)$. For each observable and each location $x = (x_l, x_t)$ an optimal number of spatial smearing steps was estimated by considering the value at which the maximum of the signal is reached. The smearing procedure also acts as an effective renormalization. This, together with the validity of our "optimal smearing step" estimation, is verified by checking the scaling of the observables in our three lattice setups (see Figure 2).

3 Perturbative field subtraction

After estimating the values of full longitudinal and transverse chromoelectric fields E_x and E_y, we need to separate it into the perturbative and nonperturbative parts. For that, we assume that the nonperturbative part is purely longitudinal

$$E_y^{\text{NP}}(x) = 0\,, \qquad E_y^{\text{P}}(x) = E_y(x)\,, \tag{4}$$

and that the curl of the perturbative part is zero:

$$\vec{\nabla} \times \vec{E}^{\text{P}} = 0\,, \qquad E_x^{\text{P}}(x_l, x_t) = \sum_{\xi=x_t}^{x_{t\max}} (E_y(x_l, \xi) - E_y(x_l + 1, \xi)\,, \tag{5}$$

where the last equation assumes also that $x_{t\max}$ is large enough that $E_x^{\text{P}}(x_l, x_{t\max})$ is negligibly small.

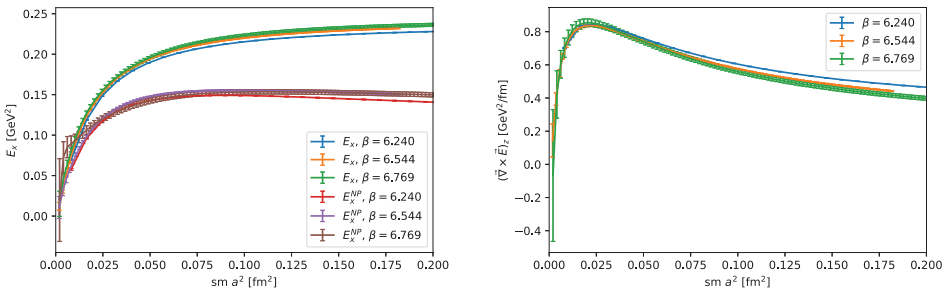

Figure 2. Dependence of the full and nonperturbative chromoelectric field at $x_l = x_t = d/2$ (left) and magnetic current density at $x_l = d/4$, $x_t = d/2$ (right) for the three different lattice setups on the number of smearing steps $sm = N_{\text{HYP3d}}$.

After finding the perturbative component, we can perform the subtraction to extract the nonperturbative component.

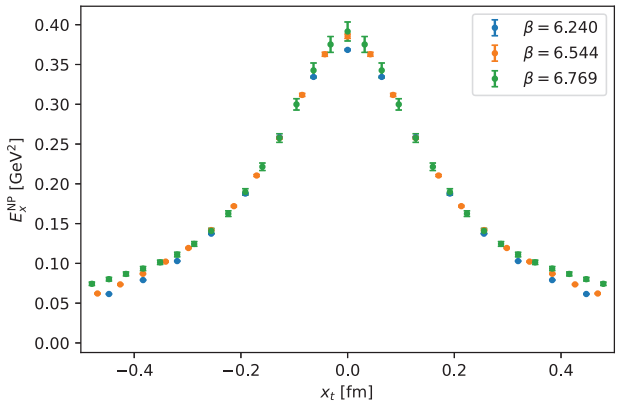

Figure 3. Continuum scaling of the longitudinal component of the non-perturbative field E_x^{NP} at a transverse plane $x_l = d/4 \approx 0.128$ fm.

4 Field derivatives in the Maxwell picture

In [39] we introduced the Maxwell stress tensor

$$T_{\alpha\beta} = F_{\alpha\lambda}F_{\beta\lambda} - \frac{1}{4}\delta_{\alpha\beta}F_{\mu\lambda}F_{\mu\lambda} \,, \tag{6}$$

and shown that the string tension $\sqrt{\sigma}$ obtained by integrating the stress tensor T_{xx} over the transverse midplane is close to the value $\sqrt{\sigma} = 0.464$ GeV, defined for our scale setting function. This implies that the main contribution to the string tension comes from the Maxwell

stress tensor, with much smaller (if any) part coming from the fluctuations in color space. Following this picture, we can write the force density in the flux tube

$$f_\beta \equiv \frac{\partial}{\partial x^\alpha} T_{\alpha\beta} = F_{\beta\lambda} \frac{\partial}{\partial x^\alpha} F_{\alpha\lambda} - \frac{F_{\mu\lambda}}{2} (\partial_\beta F_{\mu\lambda} + \partial_\mu F_{\lambda\beta} + \partial_\lambda F_{\beta\mu}) \,, \tag{7}$$

as a sum of the electric and magnetic Lorentz force densities

$$f_\beta = -F_{\beta\lambda} J^{\rm el}_\lambda - F_{\mu\lambda} \, \frac{1}{2} \epsilon_{\alpha\beta\mu\lambda} J^{\rm mag}_\alpha \,, \tag{8}$$

where

$$J^{\rm mag}_\alpha \equiv \frac{1}{2} \epsilon_{\alpha\beta\mu\lambda} \frac{\partial F_{\mu\lambda}}{\partial x^\beta}, \qquad (\epsilon_{4123} = 1) \,. \tag{9}$$

Writing the field strength tensors $F_{\mu\nu}$ in terms of $E_k = F_{\hat{4}k}$, and $B_i = \frac{1}{2} \epsilon i, j, k F_j k$ we can write the currents as

$$\begin{aligned} J_{\rm el} \equiv (\rho_{\rm el}, \vec{J}_{\rm el}) &= \left(\vec{\nabla} \cdot \vec{E}, \; \vec{\nabla} \times \vec{B} - \frac{\partial \vec{E}}{\partial x_4} \right) \,, \\ J_{\rm mag} \equiv (\rho_{\rm mag}, \vec{J}_{\rm mag}) &= \left(\vec{\nabla} \cdot \vec{B}, \; \vec{\nabla} \times \vec{E} - \frac{\partial \vec{B}}{\partial x_4} \right) \,. \end{aligned} \tag{10}$$

Taking into account the system symmetries we see $\vec{B} = 0$, $\frac{\partial \vec{E}}{\partial x_4} = 0$. That means

$$\begin{aligned} J_{\rm el} \equiv (\rho_{\rm el}, \vec{J}_{\rm el}) &= \left(\vec{\nabla} \cdot \vec{E}, 0 \right) \,, \\ J_{\rm mag} \equiv (\rho_{\rm mag}, \vec{J}_{\rm mag}) &= \left(0, \; \vec{\nabla} \times \vec{E} \right) \,, \end{aligned} \tag{11}$$

resulting in the following Lorentz force density

$$\vec{f} = \rho_{\rm el} \vec{E} + \vec{J}_{\rm mag} \times \vec{E} \,. \tag{12}$$

From the analysis in [14], we expect that the electric charge density is zero, while there could be nonzero magnetic currents. Our data supports this – electric charge density is close to zero, already a couple of lattice steps away from the sources (and the charge density close to the sources does not exhibit scaling, indicating that it is probably a lattice artifact). The rotational symmetry leaves only one possibility for the magnetic current – only $\left(J_{\rm mag}\right)_z = \frac{\partial E_y}{\partial x} - \frac{\partial E_x}{\partial y}$ can be nonzero, creating circular currents going around the system axis. The values of $\left(J_{\rm mag}\right)_z$, together with the scaling analysis can be seen in Figure 4.

Now we can finally rewrite Eq. (12) as

$$\vec{f} = -\vec{e}_y \left(J_{\rm mag}\right)_z E_x \,. \tag{13}$$

So the Lorentz force densities are directed toward the axis of the flux tube, "squeezing" the flux tube. If we divide the space by a plane that contains the tube axis, the total "confining" force F acting on one of the two halves equals

$$\begin{aligned} \vec{F} &= - \int_0^d {\rm d}x_l \int_0^\infty {\rm d}x_t \; x_t \int_{-\pi/2}^{\pi/2} {\rm d}\theta (\cos\theta \, \hat{e}_y + \sin\theta \, \hat{e}_z) f(x_l, x_t) = \\ &= -\hat{e}_y \left(2 \int_0^d {\rm d}x_l \int_0^\infty {\rm d}x_t \; x_t f(x_l, x_t) \right) \,. \end{aligned} \tag{14}$$

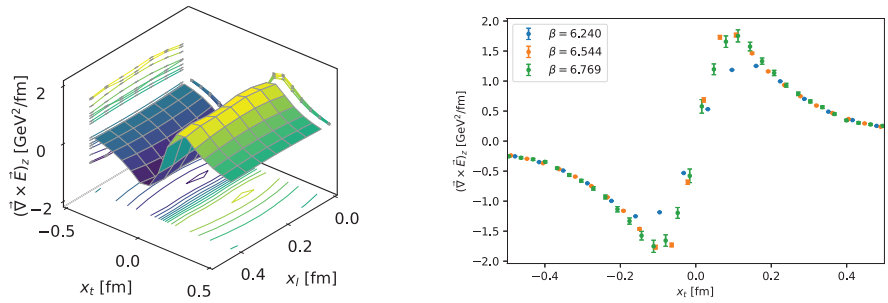

Figure 4. Spatial distribution for $\beta = 6.240$ (left) and scaling plot at a transverse plane $x_l = d/4 \approx 0.128$ fm (right) for the chromomagnetic current density J_z.

Table 2. Forces in the flux tube.

β	$\sqrt{F}$ [GeV]	$\sqrt{\sigma}$ [GeV]
6.240	$0.4859(8)^{+645}$	0.4742(15)
6.544	$0.5165(15)^{+611}_{-214}$	0.4692(23)
6.769	$0.530(4)^{+547}_{-322}$	0.467(7)

Calculating the integral in (13) numerically gives the results collected in Table 2. The systematic error estimates for $\sqrt{F}$ are obtained by taking into account the difference in the integration ranges available with the three lattice setups, and asymmetry of the extracted field, and especially current density distribution under reflection with respect to the midplane. One can see that the magnitude of the confining force F is compatible within systematic errors with the magnitude of the string tension extracted from integration of T_{xx} over the midplane. The string tension in the third column has a good agreement with the one expected for our scaling function: $\sqrt{\sigma} = 0.464$ GeV.

5 Conclusions

We have extracted the nonperturbative flux tube field from simulations of the field created by the quark-antiquark pair separated by $d = 0.511$ fm on three lattices with different gauge coupling constants (and thus different lattice spacings). The curl subtraction procedure works well even for such small distance resulting in a flux tube with a stable transverse section and a good scaling of the field values for different lattice setups. The string tension extracted from the nonperturbative field at midplane is in good agreement with the expected value.

Similar analysis of the chromoelectric charge density and the chromomagnetic current density extracted from the divergence and curl of the nonperturbative field, respectively shows that the electric charge density is close to zero at points at least a couple lattice steps away from the sources, and does not exhibit scaling close to the sources. The magnetic current density is nonzero, forming circular currents around the quark-antiquark axis.

The Maxwell picture approach employed in this work provides a good quantitative description of the fields, currents, and charges in the flux tube.

Interaction of the chromomagnetic current with the chromoelectric fields creates the Lorentz forces directed to the quark-antiquark axis. The magnitude of the total Lorentz force

acting on a half-space is compatible within systematic errors with the magnitude of the string tension.

Acknowledgements

This investigation was in part based on the MILC collaboration's public lattice gauge theory code (https://github.com/milc-qcd/). Numerical calculations have been made possible through a CINECA-INFN agreement, providing access to HPC resources at CINECA. LC and AP acknowledge support from INFN/NPQCD project. FC and VC acknowledge support by the Deutsche Forschungsgemeinschaft (DFG, German Research Foundation) through the CRC-TR 211 "Strong-interaction matter under extreme conditions" – project number 315477589 – TRR 211. FC acknowledges the support by the State of Hesse within the Research Cluster ELEMENTS (Project ID 500/10.006).

References

[1] J. Greensite, *An introduction to the confinement problem*, Vol. 821 (Springer Berlin Heidelberg, 2011)
[2] M. Fukugita, T. Niuya, Phys. Lett. **B132**, 374 (1983)
[3] J.E. Kiskis, K. Sparks, Phys. Rev. **D30**, 1326 (1984)
[4] J.W. Flower, S.W. Otto, Phys. Lett. **B160**, 128 (1985)
[5] J. Wosiek, R.W. Haymaker, Phys. Rev. **D36**, 3297 (1987)
[6] A. Di Giacomo, M. Maggiore, S. Olejnik, Phys. Lett. **B236**, 199 (1990)
[7] A. Di Giacomo, M. Maggiore, S. Olejnik, Nucl. Phys. **B347**, 441 (1990)
[8] P. Cea, L. Cosmai, Nucl. Phys. Proc. Suppl. **30**, 572 (1993)
[9] Y. Matsubara, S. Ejiri, T. Suzuki, Nucl. Phys. Proc. Suppl. **34**, 176 (1994), hep-lat/9311061
[10] P. Cea, L. Cosmai, Phys. Lett. **B349**, 343 (1995), hep-lat/9404017
[11] P. Cea, L. Cosmai, Phys. Rev. **D52**, 5152 (1995), hep-lat/9504008
[12] G.S. Bali, K. Schilling, C. Schlichter, Phys. Rev. **D51**, 5165 (1995), hep-lat/9409005
[13] A.M. Green, C. Michael, P.S. Spencer, Phys. Rev. **D55**, 1216 (1997), hep-lat/9610011
[14] P. Skala, M. Faber, M. Zach, Nucl.Phys. **B494**, 293 (1997), hep-lat/9603009
[15] R.W. Haymaker, T. Matsuki, Phys. Rev. **D75**, 014501 (2007), hep-lat/0505019
[16] A. D'Alessandro, M. D'Elia, L. Tagliacozzo, Nucl.Phys. **B774**, 168 (2007), hep-lat/0607014
[17] M.S. Cardaci, P. Cea, L. Cosmai, R. Falcone, A. Papa, Phys.Rev. **D83**, 014502 (2011), 1011.5803
[18] P. Cea, L. Cosmai, A. Papa, Phys.Rev. **D86**, 054501 (2012), 1208.1362
[19] P. Cea, L. Cosmai, F. Cuteri, A. Papa, PoS **LATTICE2013**, 468 (2013), 1310.8423
[20] P. Cea, L. Cosmai, F. Cuteri, A. Papa, Phys. Rev. **D89**, 094505 (2014), 1404.1172
[21] P. Cea, L. Cosmai, F. Cuteri, A. Papa, PoS **LATTICE2014**, 350 (2014), 1410.4394
[22] N. Cardoso, M. Cardoso, P. Bicudo, Phys. Rev. **D88**, 054504 (2013), 1302.3633
[23] M. Caselle, M. Panero, R. Pellegrini, D. Vadacchino, JHEP **01**, 105 (2015), 1406.5127
[24] P. Cea, L. Cosmai, F. Cuteri, A. Papa, JHEP **06**, 033 (2016), 1511.01783
[25] P. Cea, L. Cosmai, F. Cuteri, A. Papa, Phys. Rev. **D95**, 114511 (2017), 1702.06437
[26] E. Shuryak (2018), 1806.10487
[27] C. Bonati, S. Calì, M. D'Elia, M. Mesiti, F. Negro, A. Rucci, F. Sanfilippo, Phys. Rev. **D98**, 054501 (2018), 1807.01673

[28] A. Shibata, K.I. Kondo, S. Kato (2019), 1911.00898
[29] R. Yanagihara, T. Iritani, M. Kitazawa, M. Asakawa, T. Hatsuda, Phys. Lett. **B789**, 210 (2019), 1803.05656
[30] H. Ichie, V. Bornyakov, T. Streuer, G. Schierholz, Nucl. Phys. A **721**, 899 (2003), hep-lat/0212036
[31] P. Cea, L. Cosmai, F. Cuteri, A. Papa, PoS **LATTICE2016**, 344 (2016), 1701.03371
[32] M. Baker, V. Chelnokov, L. Cosmai, F. Cuteri, A. Papa, PoS **LATTICE2021**, 355 (2022), 2111.06618
[33] S. Chagdaa, B. Purev, E. Galsandorj, Journal of Physics G: Nuclear and Particle Physics **48**, 125001 (2021)
[34] O. Philipsen, H. Wittig, Phys. Rev. Lett. **81**, 4056 (1998), [Erratum: Phys. Rev. Lett.83,2684(1999)], hep-lat/9807020
[35] S. Kratochvila, P. de Forcrand, Nucl. Phys. Proc. Suppl. **119**, 670 (2003), [,670(2002)], hep-lat/0209094
[36] G.S. Bali, H. Neff, T. Duessel, T. Lippert, K. Schilling (SESAM), Phys. Rev. **D71**, 114513 (2005), hep-lat/0505012
[37] V. Koch, J. Bulava, B. Hörz, F. Knechtli, G. Moir, C. Morningstar, M. Peardon, PoS **LATTICE2015**, 100 (2016), 1511.04029
[38] M. Baker, P. Cea, V. Chelnokov, L. Cosmai, F. Cuteri, A. Papa, Eur. Phys. J. **C79**, 478 (2019), 1810.07133
[39] M. Baker, P. Cea, V. Chelnokov, L. Cosmai, F. Cuteri, A. Papa, Eur. Phys. J. C **80**, 514 (2020), 1912.04739
[40] Baker, M., Chelnokov, V., Cosmai, L., Cuteri, F., Papa, A., Eur. Phys. J. C **82**, 937 (2022)
[41] A. Di Giacomo, E. Meggiolaro, Phys. Lett. **B537**, 173 (2002), hep-lat/0203012
[42] S. Necco, R. Sommer, Nucl. Phys. **B622**, 328 (2002), hep-lat/0108008
[43] A. Hasenfratz, F. Knechtli, Phys. Rev. **D64**, 034504 (2001), hep-lat/0103029